HHS Public Access

Author manuscript

Rep U S. Author manuscript; available in PMC 2020 May 30.

Published in final edited form as:

Rep U S. 2019 November ; 2019: 7075–7082. doi:10.1109/IROS40897.2019.8967806.

Toward Improving Patient Safety and Surgeon Comfort in a Synergic Robot-Assisted Eye Surgery: A Comparative Study

Ali Ebrahimi[1], **Farshid Alambeigi**[1,2], **Ingrid E. Zimmer-Galler**[3], **Peter Gehlbach**[3] **[Member, IEEE]**, **Russell H. Taylor**[1] **[Life Fellow, IEEE]**, **Iulian Iordachita**[1] **[Senior Member, IEEE]**

[1]Laboratory for Computational Sensing and Robotics at the Johns Hopkins University, Baltimore, MD, 21218, USA.

[2]Department of Mechanical Engineering at the University of Texas at Austin, Austin, TX, 78712, USA.

[3]Wilmer Eye Institute, Johns Hopkins Hospital, Baltimore, MD, 21287, USA.

Abstract

When robotic assistance is present into vitreoretinal surgery, the surgeon will experience reduced sensory input that is otherwise derived from the tool's interaction with the eye wall (sclera). We speculate that disconnecting the surgeon from this sensory input may increase the risk of injury to the eye and affect the surgeon's usual technique. On the other hand, robot autonomous motion to enhance patient safety might inhibit the surgeons tool manipulation and diminish surgeon comfort with the procedure. In this study, to investigate the parameters of patient safety and surgeon comfort in a robot-assisted eye surgery, we implemented three different approaches designed to keep the scleral force in a safe range during a synergic eye manipulation task. To assess the surgeon comfort during these procedures, the amount of interference with the surgeons usual maneuvers has been analyzed by defining quantitative comfort metrics. The first two utilized scleral force control approaches are based on an adaptive force control method in which the robot actively counteracts any excessive force on the sclera. The third control method is based on a virtual fixture approach in which a virtual wall is created for the surgeon in the unsafe directions of manipulation. The performance of the utilized approaches was evaluated in user studies with two experienced retinal surgeons and the outcomes of the procedure were assessed using the defined safety and comfort metrics. Results of these analyses indicate the significance of the opted control paradigm on the outcome of a safe and comfortable robot-assisted eye surgery.

I. INTRODUCTION

Surgical tasks inside of the eye encompass manipulating delicate tissues and micron scale structures typically using instruments passing through an incision point in the sclera. In these potentially long and always delicate procedures, surgeon hand tremor and patient eye movement may cause severe injuries to the eye. The surgeon's hand tremor may happen due to physiological reasons or may be secondary to fatigue in long surgeries (an average of 182 μm was measured for an ophthalmic surgeon tremor amplitude [1]). To address these

aebrahi5@jhu.edu.

challenges and mainly with the aim of increasing patient safety, robotic manipulators and computer algorithms have been devised to synergically assist surgeons in reducing hand tremor [2].

Fig. 1 shows the key elements of a robot-assisted clinician-in-the-loop eye surgery (i.e. a surgeon, a robotic manipulator, and a target anatomy in patient). In this procedure, a robot and typically a computer algorithm synergically assist a surgeon to accurately and safely perform a particular surgical task on a patient. A review of the literature pertinent to eye surgery demonstrates that most of the research has been focused on developing robotic systems, sensorized instruments, and computer algorithms solely from the patient's perspective and have neglected the role and effect of surgeon acceptance and comfort in the outcome of a synergic robot-assisted eye surgery.

Various types of robotic systems have been designed and developed for eye surgery including collaborative robots in which surgeon and robot share the control of the surgical tool (e.g. [3], [4]), tele-manipulated robots (e.g. [5], [6]) and hand-held robotic devices (e.g. [7]). For instance, the Steady-Hand Eye Robot (SHER), as shown in Fig. 1, is an example of a collaborative robot that was fabricated at the Johns Hopkins University [8]. In addition, the first clinically-approved collaborative robots for in-human eye surgery has been designed and successfully evaluated by Edwards et al. [9] and Gijbels et al. [10]. Tele-manipulation robots have emerged as the most clinic-ready configurations for retinal surgery at this time. A master-slave intraocular robotic system capable of performing various surgical tasks was recently designed and built by Wilson et al. [6]. The University of Tokyo has also performed vitreous detachment and microcannulation using a tele-manipulated robot [5], [11]. Apart from the relatively large eye surgical robots, a hand-held device called Micron was also developed by MacLachlan et al. [7] to attenuate surgeon involuntary hand motions while maintaining the intuitive eye-hand coordination. A review of these developed systems demonstrates that they have been mostly designed to improve the outcome of the eye surgery from the patient's perspective i.e. enhancing the surgeons precision (e.g. motion scaling [5] and actively reducing tremor [7]) and/or adding hardware constraints (e.g. Mechanical remote center of motions [3]) to improve safety and outcome of surgery.

Complementary to robotic systems, computer algorithms together with sensorized instruments have been developed as assistive tools to enhance surgeon skill during eye surgery. For instance, He et al. in [12] and [13], thanks to the utilized Fiber Bragg Gratings (FBG) optical sensors, realized that using a collaborative robotic system can substantially increase the tool to eye interaction forces (i.e. sclera forces as shown in Fig. 2). Based on the reported results, this mainly happens due to the diminished perception of the sclera forces applied by the surgeon together with the robot's large inertia and mass. In response, and to ensure safe robot-assisted eye surgery, various passive and active algorithms have been implemented. For example, we provided users with a passive alerting feedback of unsafe tool to eye interaction forces via auditory feedback [14], [15]. Active force control methods have also been used to autonomously react to unsafe interaction forces during the surgery and regardless of the surgeon's motions [16], [17]. For example, in [16], our group investigated an adaptive sclera force control method to autonomously mitigate the unsafe sclera forces exerted by the the SHER during a synergic robot-assisted eye surgery. In pilot

studies with novice users, we have shown that the active force control method was more efficient than utilizing a passive audio feedback from the patient's perspective i.e. keeping the scleral forces in a prescribed lower range [16]. Similar to the methods presented, other passive and active algorithms typically neglected analysis of surgeon comfort on the outcome of the surgery and mainly have considered the patient safety as the main priority of a synergic robot-assisted eye surgery.

Here we evaluate the effect of surgeon comfort in a clinician-in-the loop robot-assisted eye surgery while also considering the patient safety. We used the SHER and performed synergic eye manipulation tasks with two expert retinal surgeons. We performed three different sets of experiments by implementing two variants of a novel adaptive force control as well as a passive directional virtual fixture approach to maintain the sclera force in prescribed safe regions. To compare the effect of these various methods on patient safety and surgeon comfort, we defined metrics and compared the obtained experimental results with the case of a control-free experiment. To the best of our knowledge, this is the first multi-objective study toward involving the surgeon's comfort in the loop of a synergic robot-assisted eye surgery.

The remainder of this paper is organized as follows. In Section II, we introduce the SHER and formulate its kinematics equations. Section III presents the utilized methods for sclera force control. Experimental setup is discussed in Section IV and results are presented in Section V. Section VI discusses the results and concludes the paper.

II. The Steady-Hand Eye Robot

The Steady-Hand Eye Robot is a 5-DoF (degrees of freedom) cooperative micro manipulator in which surgeon and robot synergically share the control of a surgical instrument rigidly being attached to the robot [8]. This collaborative robot has three translation and two rotational degrees of freedom (Fig. 2). As shown in Fig. 2, two coordinate frames associated with the robot are the spatial coordinate frame $\{S\}$, which is attached at the robot base and is fixed in the space, and the body coordinate frame $\{B\}$ which is attached to a fixed point on the tool shaft. This coordinate frame is attached at a fixed point on the tool and is rigid with respect to the robot end-effector (Fig. 2). In this paper, superscripts b and s are used to indicate a vector is expressed in $\{B\}$ or $\{S\}$, respectively.

A. Kinematics of the SHER

The SHER's kinematics can be described using the function $g_{SB}: \Theta \rightarrow SE(3)$ that maps the vector of joint angles $\Theta \in \mathbb{R}^5$ to the relative configuration of B and S, which is a matrix in $SE(3)$. This mapping can be written using product of exponential formula as following [18]:

$$g_{SB}(\Theta) = e^{\hat{\xi}_1 \theta_1} \ldots e^{\hat{\xi}_5 \theta_5} g_{SB}(0) \tag{1}$$

where $\hat{\xi}_i$ is a 4×4 matrix in $se(3)$ and θ_i is the ith element of the vector of joint angles Θ. The homogeneous transformation $g_{SB}(0)$ is the 4×4 relative configuration of S and B at $t = 0$.

For the first three translation joints ($i = 1, 2, 3$) the matrix $\hat{\xi}$ is defined as:

$$\hat{\xi}_i = \begin{bmatrix} 0_{3\times 3} & \upsilon_i \\ 0_{3\times 1} & 0 \end{bmatrix}, \text{ for } i = 1, 2, 3 \tag{2}$$

where υ_i is a unit vector showing the positive direction of ith translation joint expressed in the spatial frame at $t = 0$.

For the rotational joints ($i = 4, 5$), $\hat{\xi}$ is computed using (3):

$$\hat{\xi}_i = \begin{bmatrix} \hat{\omega}_i & -\omega_i \times q_i \\ 0_{3\times 1} & 0 \end{bmatrix}, \text{ for } i = 4, 5 \tag{3}$$

where ω_i is a unit vector representing the rotation axis of joint i at time $t = 0$ expressed in the spatial coordinate frame and q_i is an arbitrary point on this rotation axis. In both cases of (2) and (3) the matrices $\hat{\xi}_i$ can be written in twist coordinates $\xi_i \in \mathbb{R}^6$ [18]. Each twist coordinate vector ξ_i contains the directions (υ_i or ω_i) for joint i which is depicted in Fig. 2.

Considering (1)–(3), one can define the robot Jacobian (J_{SB}) relating the robot end-effector velocity to the joint velocity of the robot as following.

$$V^b_{SB} = J_{SB}(\Theta)\dot{\Theta} \tag{4}$$

where $V^b_{SB} \in \mathbb{R}^6$ is the robot velocity vector in which the first three elements and the last three elements indicate the velocity of body frame origin and the angular velocity of the body frame both expressed in frame $\{B\}$, respectively. Of note, the superscript b indicates that the elements of a vector are expressed in the frame $\{B\}$ as mentioned before. The vector $\dot{\Theta}$ is the element-wise derivative of Θ. The term $J_{SB} \in \mathbb{R}^{6\times 5}$ is the robot Jacobian:

$$\begin{aligned} J_{SB}(\Theta) &= \left[\xi_1^\dagger \ldots \xi_5^\dagger\right] \\ \xi_i^\dagger &= Ad^{-1}_{e^{\hat{\xi}_i\theta_i \ldots e^{\hat{\xi}_5\theta_5} g_{SB}(0)}}\xi_i \end{aligned} \tag{5}$$

where Ad is the 6×6 matrix of adjoint transformation depending on the configuration of the robot [18].

B. Admittance Control of the SHER

To move the robot, the surgeon holds the tool handle and maneuvers it to the desired configuration (Fig. 1). As shown in Fig. 1, a six DoF force sensor (ATI Industrial Automation, NC, USA) has been placed at the robot end-effector to measure the interaction forces and torques applied by user hand to the tool handle in the body frame. The measured vector of forces and torques, denoted by $F^b_h \in \mathbb{R}^6$, is used in a proportional admittance control algorithm, to produce intuitively natural translation and orientation motions. The utilized admittance control law, which is prior to other safety control algorithms, is defined as the following:

$$V_d^b = \mathbb{K} F_h^b \tag{6}$$

where matrix $\mathbb{K} \in \mathbb{R}^{6\times 6}$ is a diagonal matrix with constant entries on the diagonal. As it can be seen from (6), the desired velocity of the end-effector V_d^b is set to be proportional to the measured user interaction forces.

The SHER's low-level joint velocity controller is able to make the end-effector velocity $V_{SB}^b \in \mathbb{R}^6$ to follow a desired and bounded vector V_d^b calculated by (6). In other words, as shown in Fig. 3, in each sample time, the high-level controller decides the desired velocity V_d^b of the body frame and then considering (4) and (5) passes the desired joint angular velocity $\dot{\Theta}_d$ to the low-level controller as following: († denotes pseudo inverse operation)

$$\dot{\Theta}_d = J_{SB}^{\dagger}(\Theta) V_d^b \tag{7}$$

In this study, this solution (7) is obtained based on a least-square optimization formulation [19].

III. Sclera Force Control Schemes

As it can be seen from (7), the proportional admittance control provides the full control to the surgeon as it is always abiding by the surgeon's interaction force F_h^b. However, this control scheme does not consider the patient safety since it does not include the sclera interaction force feedback and therefore the surgeon may oversteps safe margins. In other words, due to the high inertia of the robot and the small interaction forces between the tool and the eyeball, surgeons are barely able to feel these interaction forces and the patient eye is prone to potential injury. To address this issue and to ensure patient safety during the SHER's control using (7), in this section, we discuss two different adaptive sclera force control methods as well as a virtual fixture approach. These safety controllers act as the outer-loop controller enforcing the desired velocity V_d^b to synergically assist surgeon performing a desired task while ensuring safety (Fig. 3). Furthermore, to investigate the effect of these safety controllers on the surgeon's comfort, we will also compare their performance in this regard.

The following sections describe the adaptive sclera force control methods. In these methods, robot regulates the sclera force autonomously and performs very small adjustments to the surgeon's movements in order to reduce the force whenever it oversteps a safe level. The third implemented method is a virtual fixture approach. This algorithm creates a virtual wall to hinder surgeon manipulation along directions toward which the sclera force will exceed safe ranges.

A. Adaptive Force Control

In a preliminary analysis with novice users, we showed that the adaptive sclera force control method is capable to guarantee the sclera force safety [16]. In this paper, we will use two

variants of this method. As shown in Fig. 3, the adaptive sclera force control is a method in which V_d^b in (6) is produced such that the components of sclera force along the x and y directions of the body frame (i.e. F_{sx} and F_{sy} in Fig. 2) will follow desired predefined trajectories $F_{dx}(t)$ and $F_{dy}(t)$ [16]. These desired reference trajectories are defined in a way to ensure safe sclera force interactions. This goal would be attained by consistently estimating the unknown robot environment compliance (i.e. unknown compliance of the tool to sclera interaction) along the x and y directions of the body frame [16]. These estimated compliances (i.e. λ_x and λ_y in Fig. 2), which are updated in each control loop using related adaptation laws, are then used as feed-forward terms together with another term coming form the tracking error of sclera force to enforce relevant entries of V_d^b. When the interaction forces overstep a predefined threshold, the adaptive sclera force control is triggered and the first two elements of V_d^b in (6) are generated according to (8) in order to make the sclera force follow desired safe trajectories. It is noteworthy to say that the last four elements of V_d^b will continue to be generated according to surgeon's interaction force (6) such that the he/she continues to synergically control the tool during manipulation.

$$\begin{aligned} V_d^b[1] &= \lambda_x \dot{F}_{dx} - k_x(F_{sx} - F_{dx}) \\ V_d^b[2] &= \lambda_y \dot{F}_{dy} - k_y(F_{sy} - F_{dy}) \end{aligned} \tag{8}$$

where the $\dot{F}_{dx}$ and $\dot{F}_{dy}$ are first derivatives of $F_{dx}(t)$ and $F_{dy}(t)$, respectively. These derivative terms multiplied by λ_x are used as feed-forward terms in the control laws. k_x and k_y are constant gains in (8).

The adaptation laws for updating the environment compliance estimations are written in (9) in which C_x and C_y are constant values.

$$\begin{aligned} \dot{\lambda}_x &= -C_x \dot{F}_{dx}(F_{sx} - F_{dx}) \\ \dot{\lambda}_y &= -C_y \dot{F}_{dy}(F_{sy} - F_{dy}) \end{aligned} \tag{9}$$

In [20], it is proved using Lyapunov method that using (8) and (9) provides force convergence for a 1-DoF system. The parameters k_x and k_y were put to be 2×10^{-6} and C_x and C_y were set to 0.1.

In the following sections, we will explain two variants of the described adaptive sclera force control being used during the conducted experiments in this paper. According to [14], the unsafe bound for sclera force was argued to be 120 mN. In order to have a safety margin, the sclera force control methods in this paper are activated in advance at 100 mN such that the robot will have enough time to prevent the sclera force from reaching 120 mN.

1) Adaptive Norm Control (ANC): In the first variant of adaptive sclera force control, we use both of the equations written in (8) *simultaneously* when the magnitude/2-norm of sclera force (i.e. $\|F_s\|_2 = \sqrt{F_{sx}^2 + F_{sy}^2}$ reaches 100 mN (time $t = t_0$). The desired trajectory for F_{sx} in this method was set to $F_{dx} = \alpha_x\left(e^{-a(t-t_0)} + 1\right)$ where α_x is half of the value of F_{sx} at t

$= t_0$ and a is set to be one. As it is apparent, the desired trajectory reduces the magnitude of F_{sx} continuously since it is a decreasing signal. By inspection it can be seen that at $t = t_0$, F_{dx} equals F_{sx} which prevents the system from having a jump after switching ON the adaptive sclera force control at $t = t_0$. A similar scenario is considered for F_{sy} and F_{dy}. Of note, this simultaneous reduction of sclera force components will also result in a reduction in the magnitude (2-norm) of the sclera force. The adaptive sclera force control is sustained until both F_{sx} and F_{sy} are reduced to 0.75 of their value at $t = t_0$.

2) Adaptive Component Control (ACC): In this method, instead of triggering both of the equations in (8), the adaptive sclera force control is *independently* switched ON for the components (i.e. F_{sx} and/or F_{sy}) that reaches 100 mN. In other words, the two equations in (8) will switch ON and OFF independently. By this method the robot provides more freedom to the surgeon since 5 components of $\dot{X}_d$ will be produced based on surgeon input force F_h^b and just one component (depending on which component of sclera force has exceeded 100 mN) will be produced according to (8). The desired sclera force trajectories would be similar to what explained in the ANC section.

B. Virtual Fixture Control

For this part, we intend to create a virtual wall for the surgeon along the component of sclera force that exceeds the safe limit of 100 mN. In other words, the robot is doing nothing autonomously and just the movement of the surgeon is blocked along the unsafe direction. By feeling a virtual wall, the surgeon will be notified that he/she is going toward an unsafe way resulting in correction the manipulation to achieve safe sclera forces. To obtain this goal, the first element or the second element of $\dot{X}_d$ (depending on whether F_{sx} or F_{sy} has reached 100 mN) are put to *zero* when the incident of exceeding 100 mN occurs and all the other five elements of $\dot{X}_d$ will be produced based on (6). Furthermore, the following logic written in (10) is implemented when having, for example, F_{sx} as the component that has exceeded 100 mN. Of note, a similar logic has been used for F_{sy}. If $F_{sx} < -100$ mN the direction of inequalities in (10) should be reversed.

$$\begin{aligned} &\text{If} \quad F_{hx}^b > 0, \quad \text{then} \quad V_d^b[1] = 0 \\ &\text{If} \quad F_{hx}^b < 0, \quad \text{then} \quad \text{use} \quad (6) \end{aligned} \tag{10}$$

where F_{hx}^b is the x component of the user interaction force in the body frame. The logic written in (10) states that if F_{sx} has exceeded 100 mN and the user is still exerting force leading in increasing F_{sx} more ($F_{hx} > 0$) the robot should stop the user from moving toward that direction $\left(V_d^b[1] = 0\right)$. If the user is applying force in opposite direction resulting in reducing F_{sx} the robot would not impede at all.

IV. Experimental Setup and Procedure

A. Experimental Setup

The setup for conducting experiments is depicted in Fig. 4 including the SHER, FBG-equipped force-sensing tool, FBG interrogator (which reads the FBG data in 1 kHz), eye

phantom and the microscope. All of the system components are connected using TCP-IP connection and the controllers are written on the main computer that runs the system. To measure sclera force components, we have utilized 80 μm-diameter Fiber Bragg Gratings (FBG) optical fibers (Technica Optical Components, China) and attached them along the tool shaft and calibrated them appropriately according to [21]. The FBG fibers are very sensitive to strain variations and have a very small diameter, which suits them for our application. The location of the FBG sensors is shown in Fig. 2. Light waves are transmitted through the fibers using the FBG interrogator (si155-Hyperion from Micron Optics Inc., Atlanta, GA), as shown in Fig. 4, and based on the variations of the wavelength of the light wave we can find the strain changes at specific points of the tool shaft. More details about the developed force-sensing tool can be found in [21]. The measurements for sclera force components, handle force and torque components and the time information for all experiments were recorded using the software package for the SHER control developed using the C++ CISST-SAW libraries [15]. The FBG-equipped sensorized tool is fixed to the tool holder of the robot wrist for manipulation (Figs. 4). To control the robot, surgeon holds the tool shaft (Fig. 1) and inserts it through the hole on the sclera of the eye phantom and manipulate the eyeball. The eye phantom, which is made from silicon, is placed under a microscope through which the surgeons should look during manipulation. The are some painted phantom vessels on the posterior of the eye phantom, which can be seen in Fig. 2.

B. Experimental Procedure

We conducted experiments with two expert eye surgeons to investigate the efficacy of the described sclera force methods. We also conducted one experiment with each surgeon without activating any sclera force control on the robot, which means the robot was purely using (6) during manipulation. Thus, for each surgeon, we performed four sets of experiments including adaptive norm control (ANC), adaptive component control (ACC), virtual fixture approach (VF) and without control of sclera force (NC). Each set of experiments was performed for 7 trials by each surgeon. The surgeons were asked to follow four specific colors with the tip of the force-sensing tool. In each experiment trial, the four color sequence changes to a new random one and is read for the surgeon to follow. As shown in Fig. 1, a secondary tool is provided to the surgeons to facilitate rotating and moving the eyeball.

C. Performance Evaluation Metrics

To investigate and evaluate the efficacy of each control method in providing patient safety and surgeon comfort, we have defined metrics to quantitatively evaluate these parameters. It is worth emphasizing that, despite the safety metric, it is extremely difficult and non-trivial to quantify the parameter of surgeon comfort with unique statistical or mathematical methods [22]. In this study, thereby considering the available force feedbacks from utilized sensors (i.e. ATI force sensor and the FBG optical fibers), we use these data to define quantitative measures as the safety and comfort metrics.

The primary variable attributed to safety analysis is sclera force values, which are analyzed in different experiment sets. The incorporated safety control methods should always ensure safe interaction sclera forces based on the defined thresholds during the surgical task. We,

therefore, can consider the percentage of experiment time spent on unsafe sclera forces ($\|F_s\|_2 > 120$ mN) as a safety metric for comparing the performance of different approaches. On the other hand, to analyze the surgeon comfort, the amount (magnitude and time) of forces/torques applied to the tool handle $\left(F_h^b\right)$ by the surgeon have been considered during the synergic robot-assisted surgical procedure. As described in the previous section, during the activation time of the safety control method, both admittance control and safety control are working together and might oppose each other depending on the interaction sclera forces. Therefore, bigger handle forces and torques during the activation times can be interpreted as the fact that accomplishing the task entails greater efforts from the surgeon which in turn attenuates comfort. Therefore, less percentage of activation time for control methods can be considered as another comfort metric.

V. Experimental Results

Tables I and II summarize the average results of the seven tasks performed by both surgeons (denoted as S1 and S2 through the paper) in each set of experiments. The reported numbers are averaged over the seven trials of each experiment. Table I reports the sclera interaction forces of each surgeon and each control method. The time information including the total time required to finish the tasks as well as the total time spent in unsafe ranges (>120mN). In addition, in the last column of Table I the averaged percent of time where that specific control is activated during experiemtns is provided. In contrast to Table I showing the average values, Fig. 5 shows the variations of sclera force magnitude versus time for a single trial of all four different methods conducted by the first surgeon. A similar plot for the second surgeon has been also shown in Fig. 6. The averaged values for the handle force magnitude and also the handle torque magnitude (the magnitude of the first three and the last three elements of F_h^b, respectively) are provided in Table II.

Figs. 7, 8 and 9 represent the sclera forces for a single trial using the ACC, ANC and VF, respectively. The stepwise lines in these plots also indicate the intervals when the adaptive control for the corresponding component has been activated or the interaction forces are higher than the desired values of 100 mN. When the line goes back to zero it means that the control is completely switched back to the admittance control as described in (7). These intervals of sclera force control activation and deactivation are denoted by T_0 and T_1 intervals in Table II, respectively. Since the ANC method controls the magnitude of sclera force, Fig. 8 only shows the 2-norm of the sclera force. On the other hand, Figs. 7 and 9 represent the independent activation/deactivation of each component. In Table II, in addition to the average value of handle force and torque over the entire experiment time, the mean value for these variables over T_0 and T_1 intervals are also provided. By providing these values we intend to see whether the surgeon is exerting bigger forces or torques while any sclera force control is activated.

VI. Discussion and Conclusion

As it can be seen from Figs. 5 and 6, when there is no sclera force control and the robot is controlled solely based on admittance control, the magnitude of sclera force grows to very

unsafe values (e.g. 5 times larger than the safe margin for surgeon 1, as shown in Fig. 5). The reason is that the surgeons have no feeling and feedback of these small forces to prevent them from happening. On the other hand, the other three control methods are functioning as they were targeted and often keeping the sclera forces in safe ranges although hops of sclera force over 120 mN limit are sometimes observed. This observation can also be deduced by looking into the averaged results in Table I. According to this table, the mean sclera force and the percent of time spent over 120 mN for the NC (No sclera force control) case are much higher than the other cases. Moreover, Table I demonstrates that the ANC method has reduced the ratio of the time spent on unsafe sclera forces for the first and second surgeon to 4% and 7%, respectively. A t-test [23] using Microsoft Excel proves that for both surgeons these percentage reductions are statistically significant with p-values less than 0.02. This indicates that the ANC method is more reliable in escalating the patient safety. This is mainly due to the fact that in this method, the robot simultaneously takes care of both components of sclera force and decreases them to safe levels. However, as summarized in Table II, for both surgeons the average of handle forces and torques in the ANC control is larger than the other control methods. This expected behavior is mainly due to the fact that in the ANC mode both of the adaptive sclera force controllers, as defined in (8), are used to simultaneously adjust the first two components of $\mathcal{V}_d^b$. Additionally, considering Table I, the amount of activation time in the ANC method is almost twice of the other approaches. Therefore, considering the higher handle loads in the activation times, as compared to the other approaches, the robot intrudes more into the surgeon motions and subsequently results in a less-comfort experience for the surgeon during the performed surgical task.

As summarized in Table I and shown in Figs. 5 and 6, the ACC approach comparing to the ANC method results in more unsafe sequences (i.e. 10% and 28% for the first and second surgeon, respectively) with p-values less than 0.05 for both surgeons. The larger incidence of unsafe interaction forces means a less-safe performance from the patient perspective. However, as reported in Table I and II, the activation time of the ACC method is almost half of the ANC approach with smaller handle forces exerted by the surgeons. Therefore, from the surgeon perspective, the ACC approach has resulted in less intrusion into the surgeon's motions and thereby a better experienced comfort during the procedure.

Another observation from Fig. 5 is the peak force created in the VF method around time t = 9 s. This is mainly due to the fact that the VF is a passive method and the robot does not have the autonomy to reduce the sclera forces. Thus, although the surgeon feels a virtual wall toward unsafe direction of the sensorized tool in his/her hand, the other assisting tool in the surgeon's left hand might affect the sclera forces of the sensorized tool even if the sensorized tool is not allowed to move by the virtual wall. This is mainly because of the compliance of the sclera environment, which may result in an inevitable force peaks in the VF method. Therefore, despite the relatively short unsafe times (i.e. 10% and 5% for surgeon 1 and 2, respectively), the occurrence of these high amplitude peaks in the interaction forces may endanger patient safety and is not favorable.

Overall considering the reported results and described performance of the implemented approaches, we can conclude that the ANC approach has better performances in terms of the

safety metric while may result in a less-comfort experience for the surgeon. On the other hand, the ACC leaded to a less-intruding performance into the surgeon's action with a higher incidence of unsafe sclera interaction forces. Therefore, we can conclude that the trade-off between patient safety and surgeon comfort and, therefore, the outcome of surgery, is the direct result of the opted control procedure in a synergic robot-assisted eye surgery.

The future work of this study includes conducting a comprehensive ex-vivo experiments with multiple surgeons to better evaluate the performance of the introduced controllers based on the defined or additional comfort metrics. For better capturing clinicians comfort, NASA TLX questionnaire will be provided [24].

Acknowledgments

This work was supported by U.S. National Institute of Health under grant number of 1R01EB023943-01 and Research to Prevent Blindness, New York, New York, USA, and gifts by the J. Willard and Alice S. Marriott Foundation, the Gale Trust, Mr. Herb Ehlers, Mr. Bill Wilbur, Mr. and Mrs. Rajandre Shaw, Ms. Helen Nassif, Ms Mary Ellen Keck, and Mr. Ronald Stiff.

References

[1]. Singhy S and Riviere C, "Physiological tremor amplitude during retinal microsurgery," in Proceedings of the IEEE 28th Annual Northeast Bioengineering Conference (IEEE Cat. No. 02CH37342). IEEE, 2002, pp. 171–172.

[2]. Channa R, Iordachita I, and Handa JT, "Robotic eye surgery," Retina (Philadelphia, Pa.), vol. 37, no. 7, p. 1220, 2017.

[3]. Gijbels A, Wouters N, Stalmans P, Van Brussel H, Reynaerts D, and Vander Poorten E, "Design and realisation of a novel robotic manipulator for retinal surgery," in Intelligent Robots and Systems (IROS), 2013 IEEE/RSJ International Conference on. IEEE, 2013, pp. 3598–3603.

[4]. Nasseri MA, Eder M, Nair S, Dean E, Maier M, Zapp D,Lohmann CP, and Knoll A, "The introduction of a new robot for assistance in ophthalmic surgery," in 2013 35th Annual International Conference of the IEEE Engineering in Medicine and Biology Society (EMBC). IEEE, 2013, pp. 5682–5685.

[5]. Ueta T, Yamaguchi Y, Shirakawa Y, Nakano T, Ideta R, Noda Y,Morita A, Mochizuki R, Sugita N, Mitsuishi M et al., "Robot-assisted vitreoretinal surgery: Development of a prototype and feasibility studies in an animal model," Ophthalmology, vol. 116, no. 8, pp. 1538–1543, 2009. [PubMed: 19545902]

[6]. Wilson JT, Gerber MJ, Prince SW, Chen C-W, Schwartz SD,Hubschman J-P, and Tsao T-C, "Intraocular robotic interventional surgical system (iriss): Mechanical design, evaluation, and master–slave manipulation," The International Journal of Medical Robotics and Computer Assisted Surgery, vol. 14, no. 1, p. e1842, 2018.

[7]. MacLachlan RA, Becker BC, Tabarés JC, Podnar GW, Lobes LA Jr, and Riviere CN, "Micron: an actively stabilized handheld tool for microsurgery," IEEE transactions on robotics: a publication of the IEEE Robotics and Automation Society, vol. 28, no. 1, p. 195, 2012. [PubMed: 23028266]

[8]. Üneri A, Balicki MA, Handa J, Gehlbach P, Taylor RH, and Iordachita I, "New steady-hand eye robot with micro-force sensing for vitreoretinal surgery," in 2010 3rd IEEE RAS & EMBS International Conference on Biomedical Robotics and Biomechatronics. IEEE, 2010, pp. 814–819.

[9]. Edwards T, Xue K, Meenink H, Beelen M, Naus G, Simunovic M,Latasiewicz M, Farmery A, de Smet M, and MacLaren R, "First-inhuman study of the safety and viability of intraocular robotic surgery," Nature Biomedical Engineering, p. 1, 2018.

[10]. Gijbels A, Smits J, Schoevaerdts L, Willekens K, Vander Poorten EB, Stalmans P, and Reynaerts D, "In-human robot-assisted retinal vein cannulation, a world first," Annals of Biomedical Engineering, pp. 1–10, 2018.

[11]. Noda Y, Ida Y, Tanaka S, Toyama T, Roggia MF, Tamaki Y,Sugita N, Mitsuishi M, and Ueta T, "Impact of robotic assistance on precision of vitreoretinal surgical procedures," PloS one, vol. 8, no. 1, p. e54116, 2013. [PubMed: 23335991]

[12]. He C, Ebrahimi A, Roizenblatt M, Patel N, Yang Y, Gehlbach PL, and Iordachita I, "User behavior evaluation in robot-assisted retinal surgery," in 2018 27th IEEE International Symposium on Robot and Human Interactive Communication (RO-MAN). IEEE, 2018, pp. 174–179.

[13]. He C, Roizenblatt M, Patel N, Ebrahimi A, Yang Y, Gehlbach PL et al., "Towards bimanual robot-assisted retinal surgery: Tool-to-sclera force evaluation," in 2018 IEEE SENSORS. IEEE, 2018, pp. 1–4.

[14]. Ebrahimi A, He C, Roizenblatt M, Patel N, Sefati S, Gehlbach P, and Iordachita I, "Real-time sclera force feedback for enabling safe robot-assisted vitreoretinal surgery," in 2018 40th Annual International Conference of the IEEE Engineering in Medicine and Biology Society (EMBC), 7 2018, pp. 3650–3655.

[15]. Cutler N, Balicki M, Finkelstein M, Wang J, Gehlbach P, Mc-Gready J, Iordachita I, Taylor R, and Handa JT, "Auditory force feedback substitution improves surgical precision during simulated ophthalmic surgery," Investigative ophthalmology & visual science, vol. 54, no. 2, pp. 1316–1324, 2013. [PubMed: 23329663]

[16]. Ebrahimi A, He C, Patel N, Kobilarov M, Gehlbach P, and Iordachita I, "Sclera force control in robot-assisted eye surgery: Adaptive force control vs. auditory feedback," in 2019 International Symposium on Medical Robotics (ISMR). IEEE, 2019, pp. 1–7.

[17]. He C, Patel N, Ebrahimi A, Kobilarov M, and Iordachita I, "Preliminary study of an rnn-based active interventional robotic system (airs) in retinal microsurgery," International journal of computer assisted radiology and surgery, vol. 14, no. 6, pp. 945–954, 2019. [PubMed: 30887423]

[18]. Murray RM, A mathematical introduction to robotic manipulation. CRC press, 2017.

[19]. Wilkening P, Alambeigi F, Murphy RJ, Taylor RH, and Armand M, "Development and experimental evaluation of concurrent control of a robotic arm and continuum manipulator for osteolytic lesion treatment," IEEE robotics and automation letters, vol. 2, no. 3, pp. 1625–1631, 2017. [PubMed: 29423447]

[20]. Roy J and Whitcomb LL, "Adaptive force control of position/velocity controlled robots: theory and experiment," IEEE Transactions on Robotics and Automation, vol. 18, no. 2, pp. 121–137, 2002.

[21]. He X, Balicki M, Gehlbach P, Handa J, Taylor R, and Iordachita I, "A multi-function force sensing instrument for variable admittance robot control in retinal microsurgery," in Robotics and Automation (ICRA), 2014 IEEE International Conference on. IEEE, 2014, pp. 1411–1418.

[22]. Giacomoni A, Concone G, Di Sandro S, Lauterio A, and De Carlis L, "The meaning of surgeon's comfort in robotic surgery," The American Journal of Surgery, vol. 208, no. 5, pp. 871–872, 2014. [PubMed: 25069634]

[23]. Montgomery DC, Design and analysis of experiments. John wiley & sons, 2017.

[24]. Hart SG, "Nasa-task load index (nasa-tlx); 20 years later," in Proceedings of the human factors and ergonomics society annual meeting, vol. 50, no. 9. Sage publications Sage CA: Los Angeles, CA, 2006, pp. 904–908.

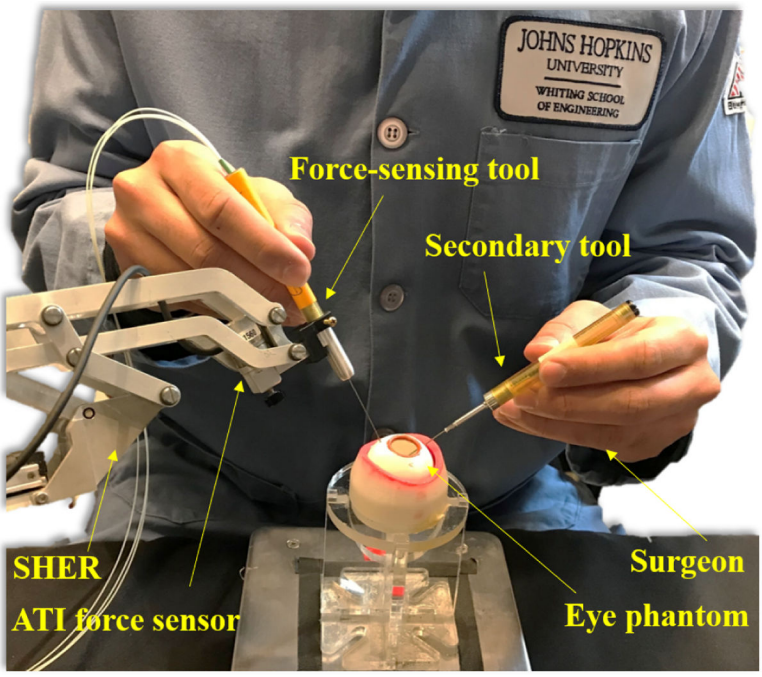

Fig. 1:

Eye phantom manipulation with the SHER– the surgeon is grabbing the force-sensing tool which is attached to the robot in the right hand and the secondary tool in the left hand to manipulate the eye phantom.

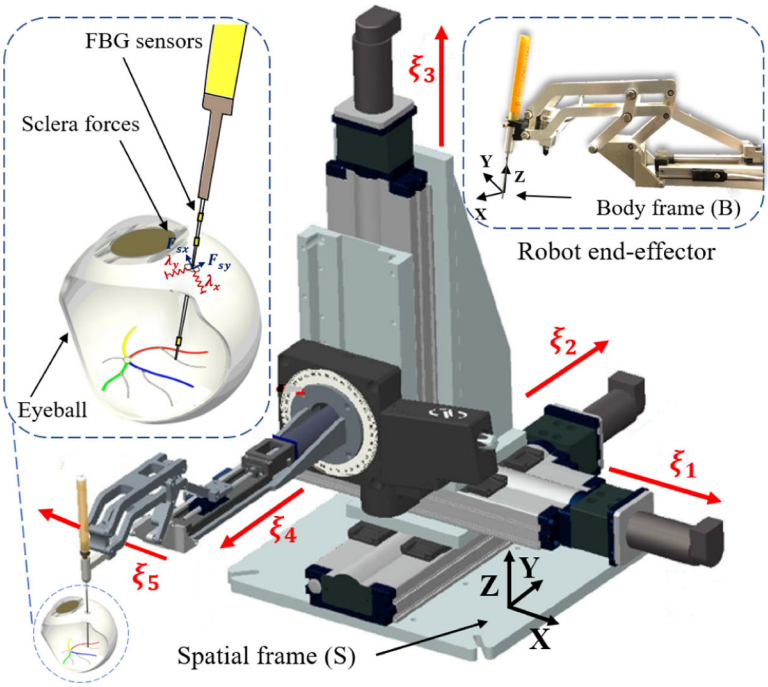

Fig. 2:

This picture shows the twist axes for the translation and rotational joints of the robot as well as spatial {*S*} and body {*B*} frames. The close-up view of the eyeball shows the sclera force components (F_{sx} and F_{sy}) and the environment compliance λ_x and λ_y. The colored phantom vessels are also visible in the eyeball.

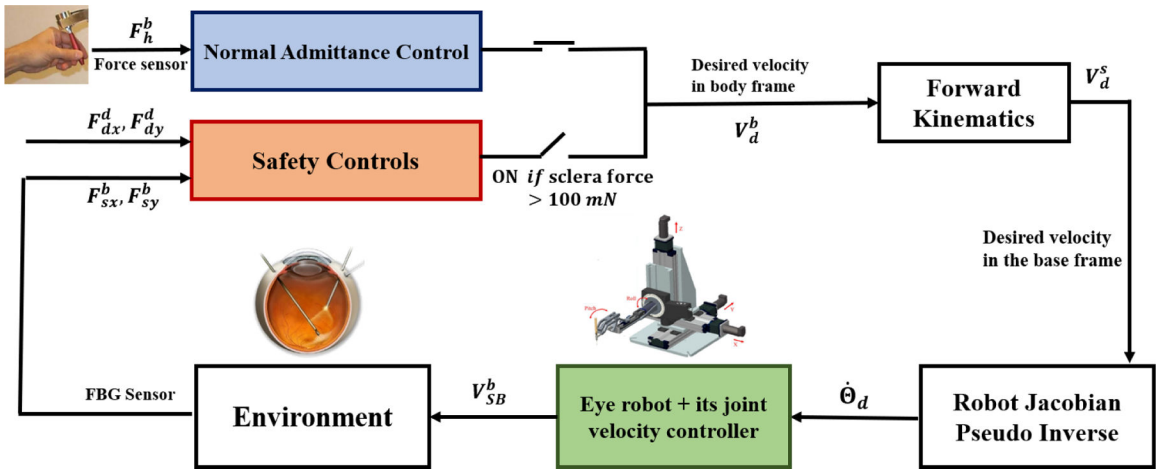

Fig. 3:

Block diagram showing the closed-loop system and 3 different control algorithms used during experiments to synergically control the SHER and ensure patient safety considering the available force feedbacks.

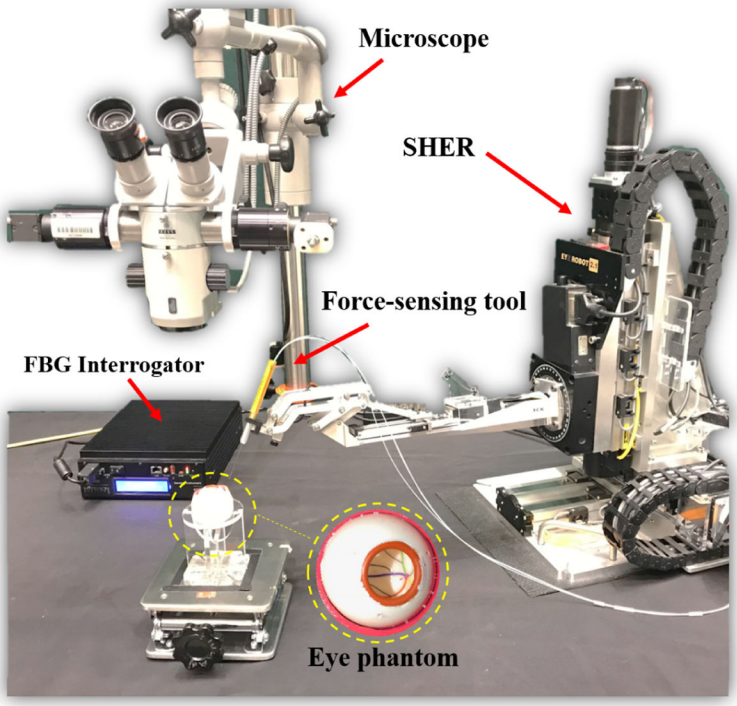

Fig. 4:
Experimental setup including the SHER, the FBG-equipped force-sensing tool, the FBG interrogator, the eye phantom and a microscope.

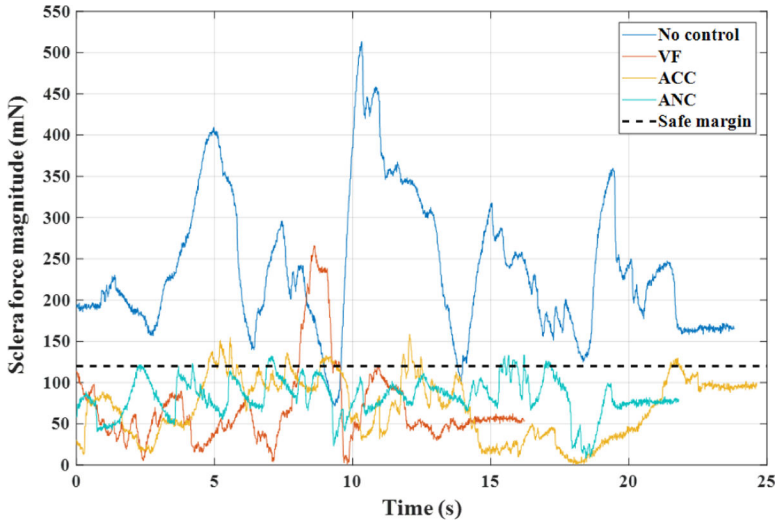

Fig. 5:

Sclera force magnitude variations for a single trial of each experiment set for the first surgeon. The unsafe threshold of 120 mN is shown in black dashed line.

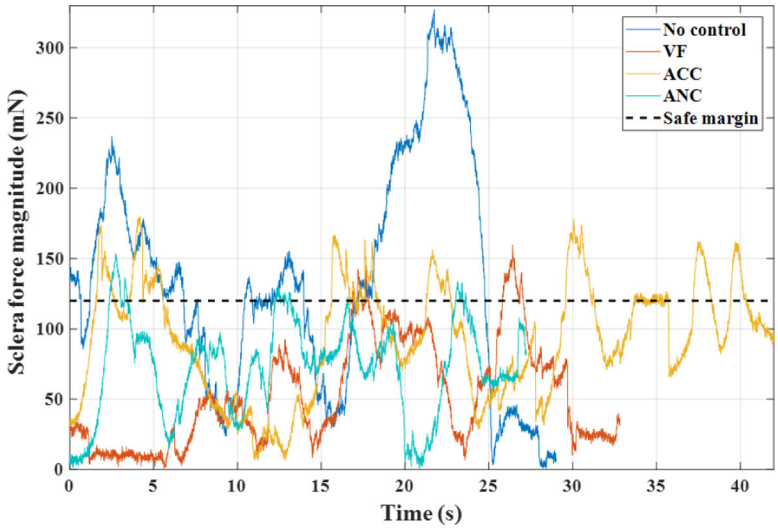

Fig. 6:

Sclera force magnitude variations for a single trial of each experiment set for the second surgeon. The unsafe threshold of 120 mN is shown in black dashed line.

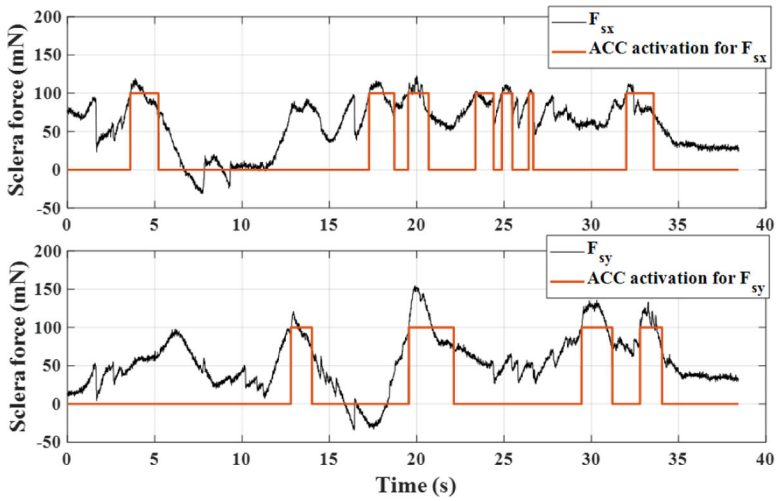

Fig. 7:

A single trial for the ACC control. The plots show the components of sclera force. The step-wise lines indicate the intervals when the adaptive control for the corresponding component is activated.

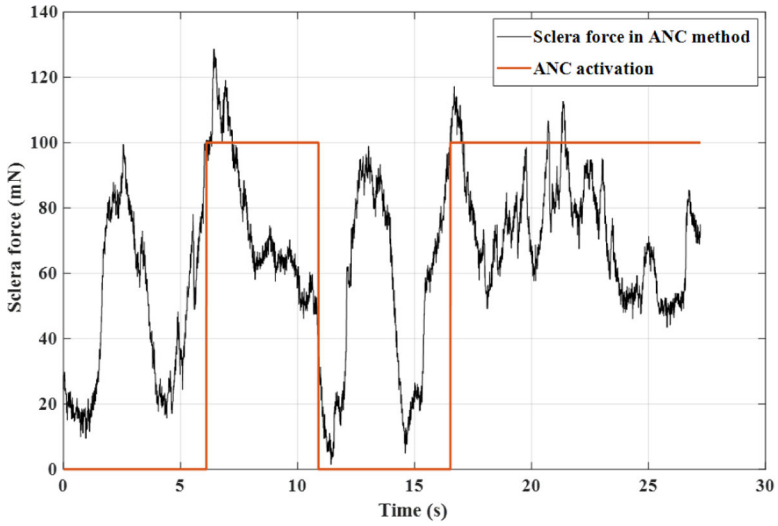

Fig. 8:

A single trial for the ANC control. The plot show the magnitude of sclera force. The step-wise lines indicate the intervals when the ANC control is activated.

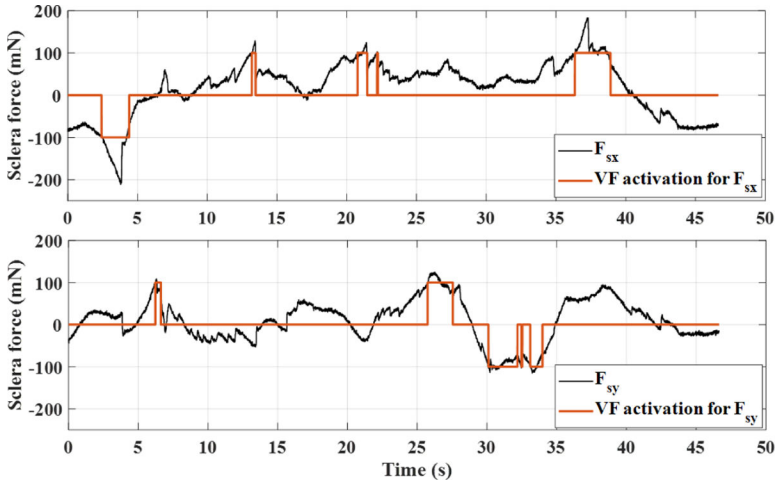

Fig. 9:

A single trial for the VF control. The plots show the components of sclera force. The step-wise lines indicate the intervals when the VF control for the corresponding component is activated.

TABLE I:

The sclera force magnitude and timing information averaged over the seven trials. The numbers in parenthesis indicate standard deviation.

S1	Mean of sclera force norm (mN)	Average total time (s)	Time over 120 mN (s)	Percent of time spent over 120 mN	Percent of activation time
NC	175.4 (87.1)	20.0 (2.8)	13.7 (5.6)	69%	--
ACC	77.27 (34.0)	30.1 (4.8)	3.2 (2.1)	10%	35%
ANC	75.47 (26.47)	23.5 (2.5)	1.0 (0.6)	4%	79%
VF	71.4 (39.00)	22.8 (6.1)	2.2 (1.1)	10%	27%
S2	**Mean of sclera force norm (mN)**	**Average total time (s)**	**Time over 120 mN (s)**	**Percent of time spent over 120 mN**	**Percent of activation time**
NC	126 (113)	28.2 (6.8)	10.9 (10.7)	38%	--
ACC	91.1 (42.92)	45.9 (5.4)	13.1 (7.2)	28%	45%
ANC	69.51 (33.24)	29.5 (4.4)	2.0 (1.6)	7%	66%
VF	62.31 (34.12)	41.8 (23.7)	1.9 (1.4)	5%	20%

TABLE II:

The Averaged results for the handle force and torque magnitudes for both surgeons.The numbers in parenthesis are standard deviation. T_0 interval is when the sclera force control is activated and T_1 is when deactivated.

S1	**Mean of handle force (N)**	**Mean of handle force over T_0 interval (N)**	**Mean of handle force over T_1 interval (N)**	**Mean of handle torque (N.m)**	**Mean of handle force over T_0 interval (N.m)**	**Mean of handle force over T_1 interval (N.m)**
ACC	0.63 (0.42)	0.72 (0.43)	0.57 (0.41)	0.023 (0.014)	0.027 (0.015)	0.021 (0.013)
ANC	0.71 (0.42)	0.68 (0.40)	0.80 (0.45)	0.030 (0.017)	0.029 (0.017)	0.031 (0.017)
VF	0.57 (0.38)	0.53 (0.35)	0.59 (0.39)	0.027 (0.014)	0.026 (0.015)	0.028 (0.014)
S2	**Mean of handle force (N)**	**Mean of handle force over T_0 interval (N)**	**Mean of handle force over T_1 interval (N)**	**Mean of handle torque (N.m)**	**Mean of handle force over T_0 interval (N.m)**	**Mean of handle force over T_1 interval (N.m)**
ACC	0.36 (0.21)	0.38 (0.22)	0.33 (0.20)	0.015 (0.007)	0.016 (0.007)	0.014 (0.007)
ANC	0.53 (0.32)	0.56 (0.40)	0.47 (0.25)	0.022 (0.012)	0.022 (0.012)	0.024 (0.011)
VF	0.36 (0.20)	0.41 (0.23)	0.35 (0.19)	0.015 (0.007)	0.015 (0.007)	0.015 (0.007)